

N-(2-hydroxyphenyl)-2-propylpentanamide, a valproic acid aryl derivative designed in silico with improved anti-proliferative activity in HeLa, rhabdomyosarcoma and breast cancer cells

Berenice Prestegui-Martel, Jorge Antonio Bermúdez-Lugo, Alma Chávez-Blanco, Alfonso Dueñas-González, José Rubén García-Sánchez, Oscar Alberto Pérez-González, Itzia Irene Padilla-Martínez, Manuel Jonathan Fragoso-Vázquez, Jessica Elena Mendieta-Wejebe, Ana María Correa-Basurto, David Méndez-Luna, José Trujillo-Ferrara & José Correa-Basurto

To cite this article: Berenice Prestegui-Martel, Jorge Antonio Bermúdez-Lugo, Alma Chávez-Blanco, Alfonso Dueñas-González, José Rubén García-Sánchez, Oscar Alberto Pérez-González, Itzia Irene Padilla-Martínez, Manuel Jonathan Fragoso-Vázquez, Jessica Elena Mendieta-Wejebe, Ana María Correa-Basurto, David Méndez-Luna, José Trujillo-Ferrara & José Correa-Basurto (2016): N-(2-hydroxyphenyl)-2-propylpentanamide, a valproic acid aryl derivative designed in silico with improved anti-proliferative activity in HeLa, rhabdomyosarcoma and breast cancer cells, *Journal of Enzyme Inhibition and Medicinal Chemistry*

To link to this article: <http://dx.doi.org/10.1080/14756366.2016.1210138>



Published online: 02 Aug 2016.



Submit your article to this journal [↗](#)



View related articles [↗](#)



View Crossmark data [↗](#)

ORIGINAL ARTICLE

N-(2-hydroxyphenyl)-2-propylpentanamide, a valproic acid aryl derivative designed *in silico* with improved anti-proliferative activity in HeLa, rhabdomyosarcoma and breast cancer cells

Berenice Prestegui-Martel¹, Jorge Antonio Bermúdez-Lugo¹, Alma Chávez-Blanco², Alfonso Dueñas-González³, José Rubén García-Sánchez⁴, Oscar Alberto Pérez-González⁵, Itzia Irene Padilla-Martínez⁶, Manuel Jonathan Fragoso-Vázquez¹, Jessica Elena Mendieta-Wejebe¹, Ana María Correa-Basurto¹, David Méndez-Luna¹, José Trujillo-Ferrara¹, and José Correa-Basurto¹

¹Laboratorio de Modelado Molecular y Bioinformática, Laboratorio de Bioquímica, Laboratorio de Biofísica y Biocatálisis, Sección de Estudios de Posgrado e Investigación, Escuela Superior de Medicina, Instituto Politécnico Nacional, Plan de San Luis y Díaz Mirón, Ciudad de México, México, ²División de Investigación Básica, Instituto Nacional de Cancerología, Tlalpan, Sección XVI, Ciudad de México, México, ³Instituto de Investigaciones Biomédicas, Universidad Nacional Autónoma de México/Instituto Nacional de Cancerología, Ciudad de México, México, ⁴Laboratorio de Oncología Molecular y Estrés Oxidativo, Sección de Estudios de Posgrado e Investigación, Escuela Superior de Medicina, Instituto Politécnico Nacional, Plan de San Luis y Díaz Mirón, Ciudad de México, México, ⁵Laboratorio de Oncología Experimental, Instituto Nacional de Pediatría, Coyoacán, Insurgentes Cuicuilco, Ciudad de México, México, and ⁶Unidad Profesional Interdisciplinaria de Biotecnología, Instituto Politécnico Nacional, Barrio La Laguna Ticomán, Ciudad de México, México

Abstract

Epigenetic alterations are associated with cancer and their targeting is a promising approach for treatment of this disease. Among current epigenetic drugs, histone deacetylase (HDAC) inhibitors induce changes in gene expression that can lead to cell death in tumors. Valproic acid (VPA) is a HDAC inhibitor that has antitumor activity at mM range. However, it is known that VPA is a hepatotoxic drug. Therefore, the aim of this study was to design a set of VPA derivatives adding the arylamine core of the suberoylanilide hydroxamic acid (SAHA) with different substituents at its carboxyl group. These derivatives were submitted to docking simulations to select the most promising compound. The compound **2** (N-(2-hydroxyphenyl)-2-propylpentanamide) was the best candidate to be synthesized and evaluated *in vitro* as an anti-cancer agent against HeLa, rhabdomyosarcoma and breast cancer cell lines. Compound **2** showed a better IC₅₀ (μM range) than VPA (mM range) on these cancer cells. And also, **2** was particularly effective on triple negative breast cancer cells. In conclusion, **2** is an example of drugs designed *in silico* that show biological properties against human cancer difficult to treat as triple negative breast cancer.

Keywords

Flexible docking, histone deacetylase inhibitors, molecular modeling, valproic acid, X-ray structure

History

Received 20 May 2016
Revised 27 June 2016
Accepted 28 June 2016
Published online 28 July 2016

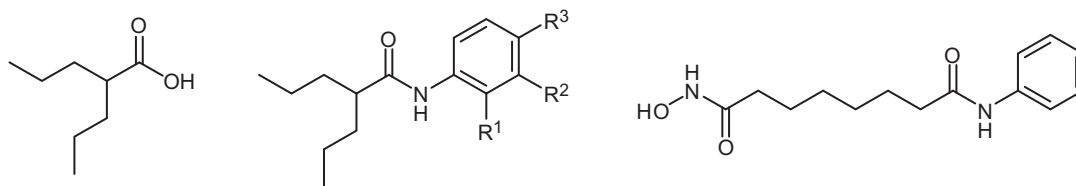
Introduction

It is thought that in the genesis of cancer there is a loss of ability to control cell proliferation, which is secondary to altered genetic material or a disruption of epigenetic processes¹. Cancer is a major cause of mortality, in 2012 there was approximately 14 million new cases and 8 million cancer-related deaths, affecting populations in all the countries and all the regions. These estimates correspond to age-standardized incidence and mortality rates of 182 and 102 per 100 000, respectively², being 3% children³. Each year, more than 160 000 children under 20

years are diagnosed with cancer in developed countries, of which 60% die⁴. Pediatric leukemia represents 30% of the pediatric cancer in which acute lymphoblastic leukemia (ALL) has had improvements in the treatment yielding well results in survival rate (90% in the latest studies) contrary to myeloid leukemia and other ALL⁵. Due to the great number of pediatric patients that die secondary to cancer disease and also, due to there are several unknown factors associated to these diseases, the European Pediatric Regulation has invited to develop drugs focused to pediatric population alongside to research programs for adults. However, there are several genetic and epigenetic factors that could represent an important genomic project to find a potential treatment or treatments in this kind of patients⁶.

Histones are octameric proteins formed by dimers of 2A, 2B, 3 and 4 subunits. In histones, the DNA material is bound and therefore, the inter-histone interactions facilitate or limit the accessibility to genes promoters in DNA, which induce or inhibit gene transcription⁷. The mechanisms include conformational

Address for correspondence: José Correa-Basurto, Laboratorio de Modelado Molecular y Bioinformática, Laboratorio de Bioquímica, Laboratorio de Biofísica y Biocatálisis, Sección de Estudios de Posgrado e Investigación, Escuela Superior de Medicina, Instituto Politécnico Nacional, Plan de San Luis y Díaz Mirón, Ciudad de México 11340, México. E-mail: jcorreab@ipn.mx



Scheme 1. Design of VPA-aryl derivatives (center) by mixing valproic acid (VPA; left) with the arylamine core of the suberoylanilide hydroxamic acid (SAHA) with different substituents (right).

changes either DNA or histones due to their post-translational modifications such as histone acetylation, methylation, phosphorylation, ubiquitination, etc., allowing that the DNA could be reached by transcription factors.

The acetylation and deacetylation of histone N-terminal Lys residues are the main regulators of interactions among histones, as well as between histones and DNA. These chemical changes are achieved by enzymes called histone acetyltransferases (HATs) and histone deacetylases (HDACs)⁸. HATs and HDACs are capable of controlling genes by activating or silencing them under dynamic processes⁹. HDACs constitute a family of zinc-dependent enzymes involved in the above processes that are divided into four main groups. Group I is comprised of isoforms 1, 2, 3, and 8, the second set includes isoforms 4, 5, 6, 7, 9, and 10 which are distributed inside either cytoplasm or nucleus; the third group (or sirtuins) are characterized by using NAD as cofactor instead of zinc; finally, group 4 contains isoform 11, which shares homology with the group 2. The catalytic site of group 1 is highly conserved, containing mainly aromatic amino acids (Phe, Tyr and Trp), an acid amino acid (Asp), and a zinc ion (Zn^{2+}); the same composition is found in group 2 which gives great structural differences as high catalytic site volume. The mechanism of removing the ϵ -amino acetyl group from Lys residues of nucleosomal histones¹⁰ is widely described.

However, there are differences among the patterns of epigenetic changes which are HDAC isoform-specific. Thus, despite of their highly conserved catalytic site, there are different residues that change their protein entrances¹¹, also, due to their cell localization which modify their natural substrate differences¹². HDACs inhibitors can suppress the activity of several HDACs by increasing the expression of specific genes related to cell morphology, metabolism, growth arrest, cell cycle arrest, differentiation, apoptosis and cell differentiation, among others^{13,14}. These HDAC inhibitors can be grouped into natural and synthetic compounds. The natural compounds include trichostatin A (TSA), apicidin, sodium butyrate, depudecin. Some synthetic compounds are pyroxamide, analogs of TSA, oxamflatin, sulfonamide hydroxamic acid, escriptaid, derivatives of phenylbutyrate and valproic acid (VPA)¹⁵. One of the most targeted HDACs is isoform 8, which is well known its role in cancer associated to epigenetic changes¹⁶. Eyal et al.¹⁷ determined the nonselective inhibition of HDACs using structural isomers of VPA. They found that 4-ene-valproic and 2-ene-valproic isomers showed IC_{50} values of 1.5 mM and 2.8 mM, respectively, compared to an IC_{50} of 1.5 mM for VPA¹⁷. Similarly, a relationship between HDAC inhibition and cytotoxicity in tumor cells was found^{18,19}. This made researchers still searching the effectiveness of VPA exploring the cell growth inhibition under apoptosis in endometrial cancer cells *in vitro* and in mice model without finding adverse effects²⁰. In addition, it has been exploited the pharmacological target of VPA under experimental procedures by comparing this drug with other more potent HDAC inhibitors, these last show limitations such as toxicity, short half-life and low bioavailability²¹.

On the other hand, suberoylanilide hydroxamic acid (SAHA) was the first FDA-approved HDAC inhibitor as anti-cancer agent that is able to induce differentiation, and/or apoptotic cell death of transformed cells *in vitro* and *in vivo*²². In addition, it is known about the role of HDAC8 and its relationship with several cancer disease, including the breast cancer^{23,24}.

The aim of the present study was to design a set of VPA aryl derivatives that maintain the SAHA core (aryl moiety) in an attempt to improve the desired inhibitory effect with low toxicity on non-tumorigenic cells. First, an *in silico* study was achieved targeting HDAC8 in tridimensional (3D) model to select those compounds that reached the catalytic site featured by Zn^{2+} atom and showed the best binding free energy values compared to VPA. We obtained a promising compound named *N*-(2-hydroxyphenyl)-2-propylpentanamide (**2**) (Scheme 1), which was chemically characterized by melting point, infrared spectroscopy (IR), nuclear magnetic resonance spectroscopy (¹H and ¹³C NMR), mass spectrometry (MS) and X-ray studies. Subsequently, this compound was tested as an anti-proliferative agent on cervical cancer (HeLa cells), rhabdomyosarcoma and breast cancer cells, where it showed higher activity than VPA.

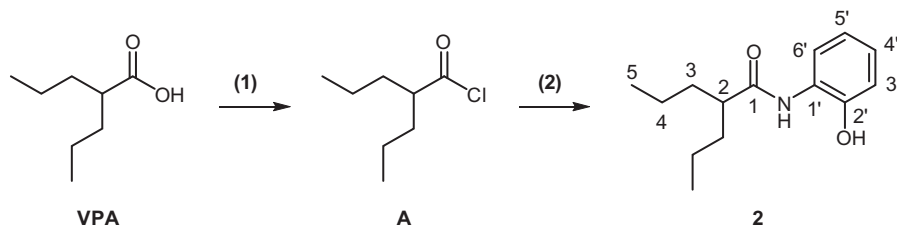
Experimental

Molecular modeling

Docking and molecular dynamics simulations

In order to evaluate the plausible molecular recognition of **2** over HDAC8 and the possible inhibitors here proposed, docking studies were carried out²⁵. Firstly, all the 2D chemical structures were drawn with IsisDraw program (<http://mdl-isis-draw.updates-tar.com/es>), submitted these structures to a previous pre-optimization of the geometry and energy at AM1 semi-empirical level, employing HyperChem software (<http://www.hyper.com/>); the complete geometrical and energetically optimization of the ligands was achieved at B3LYP6–31 level with Gaussian 98 package²⁶, the outputs Z-matrix were converted into a .pdb input file to be docked with Molekel program (<http://ugovaretto.github.io/molekel/>). Two HDAC8 crystal structures were retrieved from RCSB-PDB (ID: 1W22 and 2V5W), which were submitted them to a refinement process prior to docking simulations. Briefly, the crystal structures were stripped of additional molecules keeping the metallic atom Zn^{2+} required to catalyst process in the orthosteric binding site. Afterwards, protein structures were submitted to Molecular Dynamics simulations with NAMD2.8²⁷ running a 10 ns of total simulation under standard conditions considering a 310 K temperature and 1 ATM pressure, which were kept constant with a time step of 2 fs using the Shake algorithm²⁸ for all hydrogen atoms. Docking analysis were conducted with AutoDock4.0.1²⁹ and the used parameters were as follows: blind docking procedure with a grid box of $126 \times 126 \times 126 \text{ \AA}^3$ covering the entire orthosteric binding site into the protein, spacing between each grid point of 0.375 \AA , as scoring sampling the Lamarckian Genetic algorithm was selected

Scheme 2. Synthesis of target compound **2**. Initially, VPA reacted with oxalyl chloride to make an amide group by adding the *ortho* hydroxy aniline. Reagents and conditions: (1) oxalyl chloride and (2) *o*-aminophenol.



considering a randomized initial population of 100 individuals, and a 1×10^7 cycles as maximum number of energy evaluations.

Synthesis

Materials and methods

All chemicals (Sigma-Aldrich Química, S.A. de C.V., Toluca de Lerdo, México) and solvents (TeciQuim, S.A. de C.V., Ciudad de México, México) were of reagent grade and were used as received. Melting points (mp) was determined on an Electrothermal IA 91000 apparatus (Electrothermal, Bibby Scientific, Staffordshire, UK), these are uncorrected. IR spectra were recorded on a Perkin Elmer Frontier FT-IR spectrometer (PerkinElmer, Shelton, CT). Absorption values are expressed as the number of waves (cm^{-1}), and in the present report only the significant absorption bands are included. ^1H and ^{13}C NMR spectra were obtained on a Varian Mercury 300 MHz spectrometer (Varian, Inc., Palo Alto, CA) at 300 and 75.4 MHz, respectively, using deuterated dimethyl sulfoxide ($\text{DMSO-}d_6$) as the solvent. Electrospray Ionization (ESI) high resolution MS was performed with a Bruker micrOTOF-Q II instrument (Bruker Daltonik GmbH, Bremen, Germany).

N-(2-hydroxyphenyl)-2-propylpentanamide (**2**)

Oxalyl chloride (3.71 mL, 34.6 mmol) was added dropwise to VPA (5 g, 34.6 mmol) at 0°C . The reaction mixture was stirred for 8 h at the same temperature; then, it was allowed to warm at room temperature under nitrogen to give 2-propylpentanoyl chloride (**A**) (Scheme 2). The flux of nitrogen was continued for 15 min and was suspended for 15 min; this alternated process was carried out for 3 h, followed by cooling at -5°C . Hexane (3 mL) and *ortho* hydroxy-aniline (3.74 g) were added and the mixture stirred for 12 h before adding hexane (10 mL) and sodium bicarbonate (3 g); subsequently, the mixture was stirred for 3 h. The compound was obtained by distillate hexane extraction and the solid formed was filtered and washed with hexane. The synthesis of the compound was monitored by thin layer chromatography using a hex/AcOEt (8:2) mixture as the eluent, obtaining **2** as a white solid in 85% yield. White solid, $R_f=0.45$ (Hex/AcOEt 8:2), $\text{mp}=56 \pm 2^\circ\text{C}$. FT IR (ATR) ν_{max} 3260, 3128, 3071, 2959, 2930, 2866, 1631, 1545, 1499, 752 cm^{-1} . ^1H NMR (300 MHz, $\text{DMSO-}d_6$) δ 9.73 (br, 1H, OH), 9.37 (s, 1H, NH), 7.60 (d, $J=3$ Hz, 1H, H-6'), 6.95 (t, $J=3$ Hz, 1H, H-5'), 6.85 (d, $J=6$ Hz, 1H, H-3'), 6.76 (t, $J=6$ Hz, 1H, H-4'), 2.58 (q, $J=3$ Hz, 1H, H-2), 1.55–1.50 (m, $J=3$ Hz, 2H, H-3), 1.36–1.24 (m, 6H, H-3, 2H-4), 0.87 (t, $J=3$ Hz, 6H, 2H-5). ^{13}C NMR (75.4 MHz, $\text{DMSO-}d_6$) δ 175.5 (C-1), 148.7 (C-2'), 126.8 (C-1'), 125.4 (C-4'), 123.1 (C-6'), 119.5 (C-5'), 116.7 (C-3'), 46.0 (C-2), 35.5 (2C-3), 20.7 (2C-4), 14.5 (2C-5). ESI-MS calculated for $\text{C}_{14}\text{H}_{21}\text{NO}_2$: $[\text{M} + \text{Na}]^+$ 258.1470. Found: 258.1482.

X-ray diffraction

Single crystal of **2** was ground by slow crystallization from hexanes. The X-ray data were collected on a Bruker D8 Venture

Table 1. X-ray data, collection and refinement parameters for **2**.

Empirical formula	$\text{C}_{14}\text{H}_{21}\text{NO}_2$
Formula weight	235.32
Size (mm)	0.14X0.19X0.51
Crystal system	Monoclinic
Space group	$\text{P2}_1/\text{c}$ (No. 14)
a (Å)	8.0515(4)
b (Å)	9.0833(4)
c (Å)	19.0559(10)
α ($^\circ$)	90
β ($^\circ$)	98.740(2)
γ ($^\circ$)	90
V (Å ³)	1377.45(12)
ρ_{calcd} (g/cm^3)	1.135
Z-value	4
μ (mm^{-1})	0.075 (Mo K_α)
T (K)	173(2)
$2\theta_{\text{range}}$ ($^\circ$)	4.978–50.57
Total reflections	11053
Unique reflections	2512
R_{int} (%)	6.83
$I > 2\sigma(I)$	1767
Parameters	156
Goodness of fit	1.107
R (%), R_w (%)	5.75, 19.51
ρ_{min} , ρ_{max} ($\text{e}^- \text{Å}^{-3}$)	−0.59, 0.67
CCDC deposition	1429149

diffractometer (Bruker AXS GmbH, Karlsruhe, Germany) equipped with Mo- K_α radiation ($\lambda=0.71073$ Å). The frames were integrated with the Bruker SAINT Software package using a narrow-frame algorithm. Data were corrected for absorption effects using the multi-scan method SADABS³⁰. The final anisotropic full-matrix least-squares refine on F^2 . The structure was solved by direct methods using SHELXS-2013³¹ of the WINGX package³². The final refinement was performed by full-matrix least-squares methods using the SHELXL-2013³¹ program. Crystal data, collection and refinement parameters are given in Table 1. H atoms on C, N, and O were positioned geometrically and treated as riding atoms with: C–H 0.95–0.99 Å, $\text{Uiso}(\text{H})=1.2$ eq(C) or 1.5 eq(C); O–H = 0.84 Å, $\text{Uiso}(\text{H})=1.5$ eq(O); N–H = 0.88 Å, $\text{Uiso}(\text{H})=1.2$ eq(N). Platon³³ and Mercury³⁴ were used to prepare the material for publication. Data collection and refinement parameters, atom coordinates, bond lengths and bond angles have been deposited with the Cambridge Crystallographic Data Center. The CCDC deposition number is 1429149.

Biological evaluation

Cell cultures

Cancer cell lines HeLa (cervical cancer), MCF-7, MDA-MB-231, SKBr3, MCF-10A (breast), A204 (rhabdomyosarcoma) were obtained from ATCC, whereas Human Umbilical Vein

Endothelial Cells (HUVEC) were from primary culture. HUVEC were isolated from umbilical cord according to a previously described procedure³⁵. Cells were grown in M199 media with 1% endothelial cell growth supplement, heparin, and 15% fetal bovine serum. The donor of umbilical cord was recruited at the Hospital Juarez of Mexico. The Ethics and Research Committee of the Hospital Juarez of Mexico approved the participation of the donor and a written informed consent was obtained.

HeLa and A204 cells were cultured in DMEM medium (Gibco Lab, Grand Island, NY) in 5% bovine fetal serum. MCF-7 and MDA-MB-231 cells were preserved in DMEM high glucose (4.5 g/L) medium with phenol red, 5% bovine fetal serum and antibiotic 1X (streptomycin/penicillin 10000 U/mL, Gibco Lab, Grand Island, NY). MCF-10A cells were cultured in DMEM/F12 medium without phenol red and SKBR3 were cultured in DMEM/F12 with 10% bovine fetal serum. Cells were incubated at 37 °C in a humid atmosphere of 5% CO₂, keeping the environment at physiological pH.

In order to corroborate the biological effects of VPA (positive control) and explore those of **2**, cell cultures were used to study cytotoxicity. For this purpose, **2** was evaluated in HeLa cells at the same concentrations reported for VPA in this cell line.

Cell antiproliferative activity assays

Cervical cancer (HeLa) and rhabdomyosarcoma (A204) cell line. The effect of **2** and VPA on cell proliferation was measured with the tetrazolium salt WST-1. First, 10⁴ cells were plated in 96-well plates and incubated for 24 h (37 °C, 5% CO₂) to allow them to adhere to the plate. Then different concentrations of the drug solutions (**2** and VPA) were prepared (from the stock solution) and added to the culture medium to treat the cells for 24 h. Subsequently, the content of each plate was aspirated and 100 µL of culture medium and 10 µL of WST-1 were added, followed by incubation for 4 h. Then, the plates were read with an ELISA plate reader at 520 nm. The IC₅₀ was calculated by testing different drug concentration-responses, plotting the values, and making a curve on the University of Tokyo server (<http://bsmdb.tmd.ac.jp/3000/>) through a logarithmic analysis of four variables.

Furthermore, cell proliferation was measured by the 3-(4, 5-dimethylthiazol-2-yl)-2,5-diphenyltetrazolium bromide (MTT) assay. Cells were treated as aforementioned and at the end of the experimental period the medium was removed and replaced with 100 µL of medium with MTT (0.5 mg/mL), but without phenol red, and incubated for 2.5 h. Then, the medium was removed and replaced with 150 µL of DMSO. Optical density was measured at 550 nm in a spectrophotometer (Sinergy Biotek Instruments, Winooski, VT).

Breast cancer cell lines. Initial concentrations used in this study were determined based on the previous results obtained from the logarithmic curve. A 25 mM stock solution of **2** was prepared in dimethyl sulphoxide (DMSO) and a 25 mM stock solution of VPA in phosphate buffer solution (PBS). MCF-7 (ER+, PR+ and HER2+), MDA-MB-231 (ER-, PR- and HER2), SKBr3 (ER-, PR-, HER2+, GPER+) and MCF-10A (benign) cells were treated with 800 µL of trypsin 0.05% (Invitrogen, Waltham, MA) and counted with a Neubauer camera.

Each cell line was placed in 96-well plates at a density of 1 × 10⁴ cells per well and incubated overnight. Seven different concentrations were prepared by dilution of the stock solution: 100 µM, 150 µM, 200 µM, 250 µM, 300 µM, 350 µM and 400 µM. Cells were treated at each concentration for 24, 48, and 72 h. Each concentration/time was tested in quadruplicate. The assay for the determination of IC₅₀ was performed in triplicate.

The IC₅₀ was calculated by testing different drug concentration-responses, plotting the values, and building a curve in

Graphic Prism program V.6.0, through a logarithmic analysis of four variables. The statistical analysis was realized with *t* de student test, considering a *p* values of 0.05 difference significance statistical, for comparative anti-proliferative effect between compound **2** and VPA.

Results and discussion

Molecular modeling

Docking simulations of VPA aryl derivatives on HDAC8

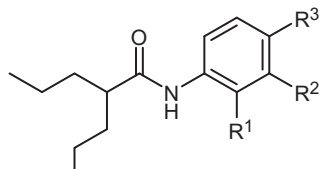
The theoretical studies show several advantages during the development of new chemical entities with potential biological activity on a determinate target, such as those implicated in cancer. Based on the chemical knowledge of the ligands and/or their targets, it is possible to design molecules from combining different pharmacophores able to reach different sites of the same protein or distinct proteins (bi-target or multi-target compounds), which could improve the anti-proliferative effect *in situ*, and consequently, in the improvement of the treatment efficiency³⁶.

In this work, we focused on the design and evaluation of a set of VPA aryl derivatives with the aim of increasing the biological potency of this drug, thus an aryl moiety was included at the carboxyl group of VPA to get certain similarity with the aryl core of SAHA molecule (Scheme 1), being the common target of these pharmacophores the HDAC8, since it has been shown that this protein has several binding sites of recognition²¹. Once the ligands were designed, they were submitted to docking simulations on previously reported HDAC8 structures (PDB code: 1W22 and 2V5W), and using the methodology previously reported for exploring the VPA recognition pattern on HDAC8 conformations³⁷. Hence, the parameters used to select the best compounds, were the free energy values (Table 2) and the binding pose. The interaction of VPA aryl derivatives on HDAC8 in the docking simulations showed that the compounds **2**, **18**, **19**, **20** and **21** had the better affinity values (Figure 1), which were favored by certain types of chemical substituents and their structural conformation adopted through docking. Furthermore, these parameters have shown certain relationship with experimental data (K_i of HDAC1: 0.4 mM)³⁸.

We decided to conduct a search for the binding properties of VPA with a region of the HDAC protein that Vannini et al. described in 2007 as the acetyl shuttle site (ASL), which was removed during catalysis³⁹. This region is close to the stearic site, in connection with it through a narrow passage that is probably responsible for removing the reaction product. In this search we found that there was a tendency of VPA to have higher affinity for this ASL site than for the catalytic site in HDAC8³⁷, and vice versa when VPA was tested with HDAC1, 2, and 3. For the members of Class II, the location or existence of this acetate release site is not clear. Based on this analysis, we proceeded to search the drug library for other activity against HDAC8. We considered the aryl moiety of SAHA due to its structural stability in the HDAC8 aromatic environment, in which Tyr100 serves to engage the ligand in the protein-binding site^{40,41}.

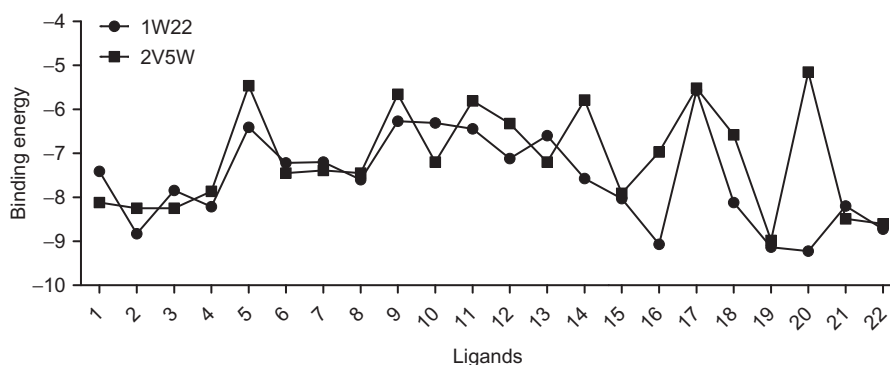
As can be seen, regardless of the substitution in each compound, the orientation in space of the catalytic site is very similar (Figure 2, below). This is because the aliphatic chains stabilize the compound in the inlet of the throat of the catalytic site in all the cases, whereas the aromatic moiety reaches certain residues (as occurs for example with SAHA). The difference in the affinity values depends on the type and amount of weak interactions caused by the substituted chemical group, which interacts electrostatically with the zinc atom in HDAC8, thus providing this protein with a partial negative charge (Figure 2, left). In the current contribution, the VPA aryl derivatives show a

Table 2. Free energy values of the VPA aryl derivatives coupled on two crystal structures of HDAC8 retrieved from the protein data bank (PDB) obtained by docking studies.



Ligand	R ¹	R ²	R ³	PDB ID: 1W22	PDB ID: 2V5W
VPA	—	—	—	-7.27	-7.0
1	H	H	H	-7.41	-8.12
2	OH	H	H	-8.83	-8.25
3	H	OH	H	-7.84	-8.25
4	H	H	OH	-8.21	-7.86
5	OCH ₃	H	H	-6.41	-5.46
6	H	OCH ₃	H	-7.22	-7.45
7	H	H	OCH ₃	-7.2	-7.39
8	F	H	H	-7.6	-7.45
9	H	F	H	-6.27	-5.66
10	H	H	F	-6.31	-7.2
11	Cl	H	H	-6.44	-5.81
12	H	Cl	H	-7.12	-6.32
13	H	H	Cl	-6.6	-7.2
14	NO ₂	H	H	-7.57	-5.79
15	H	NO ₂	H	-8.03	-7.91
16	H	H	NO ₂	-9.07	-6.97
17	CO ₂	H	H	-5.57	-5.52
18	H	CO ₂	H	-8.12	-6.58
19	H	H	CO ₂	-9.13	-8.98
20	NH ₂	H	H	-9.22	-5.15
21	H	NH ₂	H	-8.2	-8.49
22	H	H	NH ₂	-8.72	-8.6
TSA	—	—	—	-8.92	-8.39

Figure 1. Relationship of the binding energy (kcal/mol) of each compound tested in the two crystal structures of HDAC8.



binding pose behavior different than that observed for the lead compound³⁷. This means that the aryl addition induced a SAHA binding site recognition, which explains the better affinities for the derivatives compared to that observed for VPA.

Hence, based on docking results, it was shown that the compound *N*-(2-hydroxyphenyl)-2-propylpentanamide (**2**) is one of the most promissory compounds according to its free energy values and non-bond interactions.

Chemistry

Compound **2** was successfully synthesized in 85% yield by chlorination of valproic acid (VPA) with oxalyl chloride to form 2-propylpentanoyl chloride (**A**) and subsequent amidation with ortho hydroxy aniline (Scheme 2). Analytical data are in

agreement with the proposed structure, particularly, amide NH and phenolic OH are observed at 9.37 and 9.73 ppm in ¹H NMR spectrum and carbonyl appears at 175.5 ppm and at 1631 cm⁻¹ in ¹³C NMR and IR spectra, respectively.

Compound **2** gave single crystals suitable for X-ray diffraction analysis, the corresponding structure is shown in Figure 3 and selected geometric parameters are listed in the captions. Bond lengths and angles are characteristics of the amide bond. The structure of **2** in the crystal is very similar to that adopted in the high affinity conformation of HDAC obtained from docking. In both cases, the amide group is out of the mean phenyl plane with O(17)C(8)N(7)C(1) and C(2)C(1)N(7)C(8) torsion angles of 11.1(4) and -44.2(3) in the crystal and 0.06 and -82.01 in the docked conformation, respectively. In this last, the OH group is twisted to the anti-conformer by hydrogen bonding with Tyr306

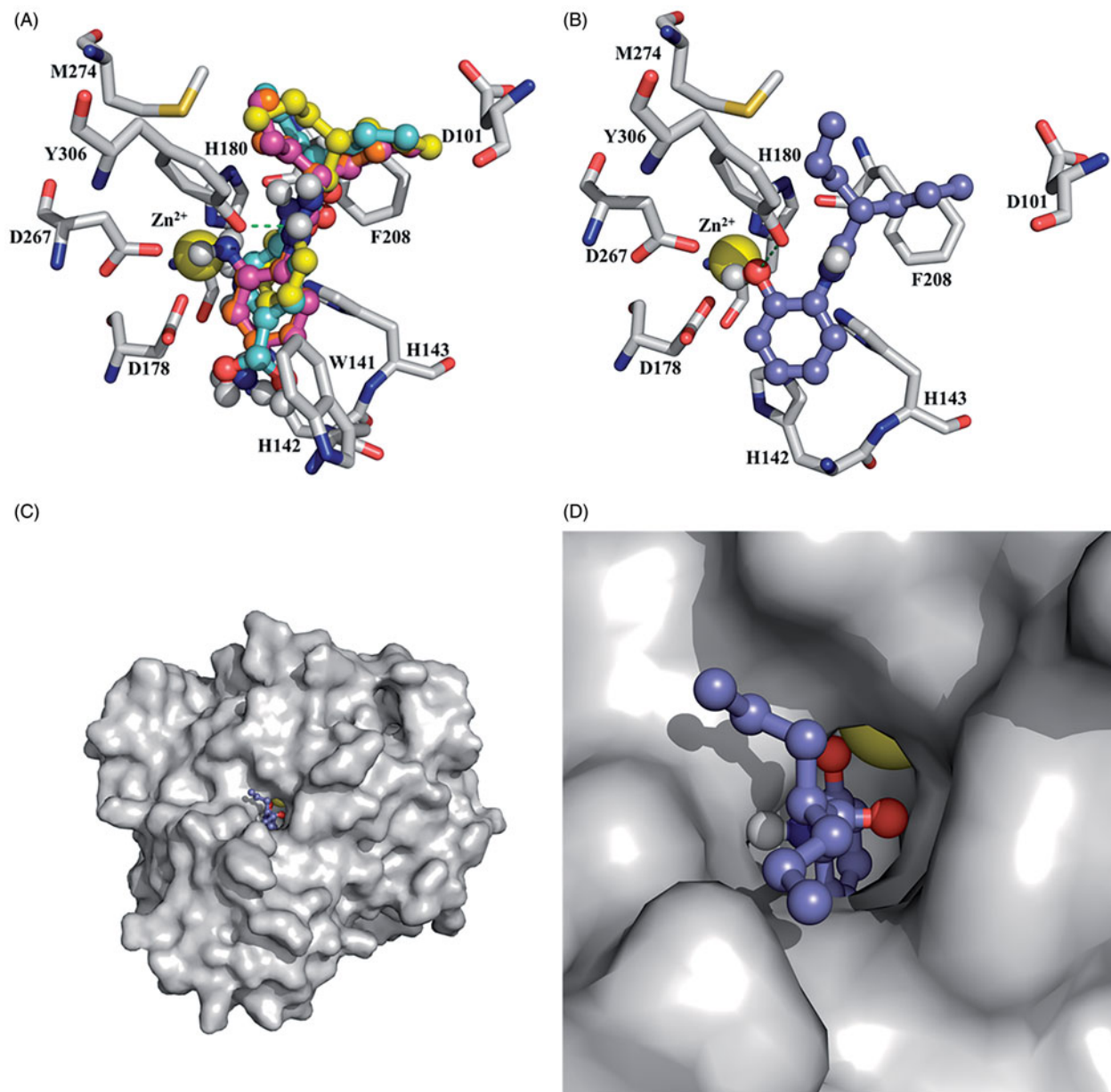


Figure 2. Interactions of compound 2, 18, 19, 20 and 21, (A) all ligands are capable of adopting the same binding pose. (B) 2 is making a coordination with Zn^{+2} . (C) and (D) show the cavity of HDAC8 reached by the target ligands.

of HDAC binding site, whereas in the crystal the OH is syn positioned to the benzene ring. The $OH \cdots O$ hydrogen bonding between phenolic donor and carbonyl amide acceptor, gives shape to a helix type structure in the crystal.

Biological activity

In vitro antiproliferative activity of 2 on cervical cancer cells (HeLa)

After standardizing the management of the cell line, we proceeded to obtain information of the effect of **2** comparing this with that of VPA. A concentration response curve was constructed under logarithmic units (100 mM to 1×10^{-3} mM for VPA, 10 mM to 1×10^{-4} mM for **2**) by measuring the percentage of cell viability. The sigmoid curves reflect the concentration-dependent effect of both compounds based on the decrease of cell viability determined by the MTT assay (Figure 4A). Compound **2** proved to be 10 times more potent than VPA. With the curve, it was possible to calculate the IC_{50} on HeLa cells for each

compound, resulting in 0.92 mM for **2** and 9.12 mM for VPA. The IC_{50} value for VPA was calculated as previously reported using a concentration 3 mM^{42} .

Once obtaining the IC_{50} for each drug, we seeded 1×10^6 cells in 25 mL culture flasks, each with 5 mL of DMEM medium (alone or in combination with the IC_{50} of one of the drugs). We made a photographic follow-up of both time and effect. Whereas there was an increase in the number of cells in the control, the cells in the flasks with **2** and VPA maintained the same level from 0 to 24 h (data not shown). This can be explained by a cytostatic effect or a certain degree of apoptosis induced by the drugs. Subsequently, an assay was conducted to detect apoptosis in order to clarify the type of cell death that each drug caused. We used an apoptosis detection kit (Takara Inc.) to evaluate cellular DNA cut by endonucleases (typical of the apoptotic process but not of necrosis). Fragmented DNA is identified by adding TdT (terminal deoxynucleotidyl transferase), which complements the chains on any 3'OH found. The nucleotides used are marked with fluorescein and later stimulated with UV light. The control cells (untreated cells) were observed in red, showing no fluorescence.

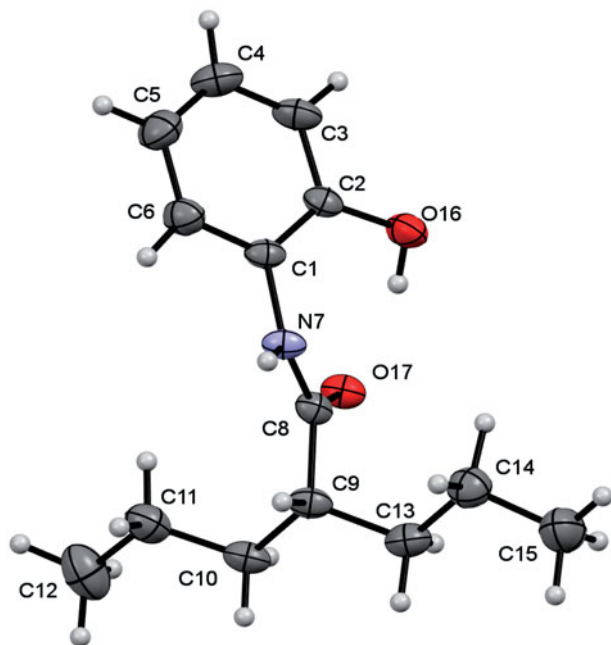


Figure 3. Molecular structure of compound **2**. Selected geometric parameters: bond lengths (Å): O(2)–C(2) 1.366(3), O(17)–C(8) 1.245(2), N(7)–C(1) 1.426(3), N(7)–C(8) 1.337(3); bond angles (°): C(1)–N(7)–C(8) 127.36(17), O(2)–C(2)–C(1) 123.3(2), O(2)–C(2)–C(3) 117.7(2), O(17)–C(8)–N(7) 122.0(2), O(17)–C(8)–C(9) 120.81(19), N(7)–C(8)–C(9) 117.23(17); torsion angles (°): C(2)–C(1)–N(7)–C(8) –44.2(3), N(7)–C(1)–C(2)–O(2) –3.3(3), O(17)–C(8)–N(7)–C(1) 11.1(4), C(9)–C(8)–N(7)–C(1) –167.9(2), O(17)–C(8)–C(9)–C(10) –59.7(3), O(17)–C(8)–C(9)–C(13) 65.4(3), N(7)–C(8)–C(9)–C(13) –115.6(2).

Whereas some slightly positive cells were found when using the IC_{50} of **2** and VPA (in a time-dependent trend: 24 h < 48 h), the fluorescence was intense (more seen in the nucleus) when the IC_{99} concentration was employed for 4 h, indicating a strong apoptotic response (data not shown).

In vitro antiproliferative activity of **2** on rhabdomyosarcoma (A204) cell line

Assays were conducted with the rhabdomyosarcoma (A204) cell line to identify the activity of **2** and VPA. Since doxorubicin is known to have activity against this type of tumor, it was added as a positive control. Compound **2** and doxorubicin had a similar profile on cell growth inhibition, while VPA showed approximately 100 times less potency (Figure 4B). The concentration-response curves were created with the University of Tokyo server to obtain the IC_{50} concentration for each compound: 36.42 μ M for **2**, 12.25 mM for VPA, and 12.22 μ M for doxorubicin.

In vitro antiproliferative activity of **2** on breast cancer cell lines

MCF-7, MDA-MB-231, SKBr3, endothelial (Human Umbilical Vein Endothelial Cells (HUVEC) and MCF-10A cells were either untreated or treated with different concentrations of **2** and VPA for 72 h (0–350 μ M). After this time, it was found that the concentrations of **2** that were employed suppressed MCF-7 cell proliferation in a concentration-dependent manner, with the highest concentration decreasing cell to 20.8% of that found in the control cells (Figure 5A; $p = 0.001$). However, with VPA cell proliferation was maintained at about 100% regardless of the concentration. A similar effect was observed in MDA-MB-231 cells treated for 72 h (Figure 5B), with 400 μ M of **2** decreasing cell proliferation to 8.7% ($p = 0.003$), and VPA showing virtually no effect.

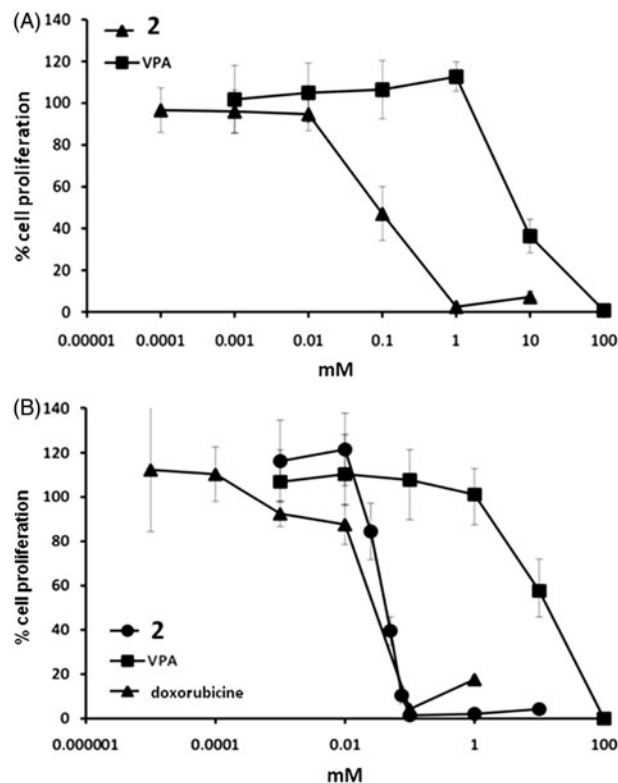


Figure 4. (A) Concentration-response curve of VPA and **2** in HeLa cells. (B) Concentration-response curve of VPA and **2** in the A204 cell line. All data on cell proliferation after treatment are expressed as the percentage of cell growth of treated versus untreated (control) cells. All assays were determined by WST.

Endothelial and MCF-10A cell lines (non-tumorigenic) were used as a control because they are considered normal epithelial cells. The effect of **2** was assayed at the same concentrations previously used. With 250 μ M of compound **2** ($IC_{50} = 213.7 \mu$ M), at 72 h of treatment cell proliferation decreased to 11.3% of that found in the control cells (Figure 5C). This result indicates that normal breast cells were more sensitive than breast cancer cell lines.

When we treated SKBr3 cells with **2**, a higher inhibitor effect on cell proliferation was found than with the other cell lines. Hence, we used lower concentrations (0–250 μ M) to find the IC_{50} . VPA did not have any inhibitory effect. Rather, we observed a slight increase in cell proliferation at the highest concentrations used (Figure 5D).

The IC_{50} values of **2** were the following: 192.4 μ M for MCF-7 cells, 283.0 μ M for MDA-MB-231 cells, 213.7 μ M for MCF-10A cells, and 142.0 μ M for SKBr3 cells. As reported in Table 3, **2** exhibits cytotoxic activity on all cell lines. This compound showed activity at concentrations that could be considered clinically acceptable. In contrast, at the same concentrations VPA was not able to exert an effect on breast cancer cell lines. These results suggest that **2** is capable of inhibiting cell growth of estrogen responsive cells, with the greatest effect found in the SKBr3 cell line.

It is known that there are reports in which VPA exerts its inhibitory activity of HDACs at concentrations higher than those found herein. In 2007, Fortunati et al. reported an IC_{50} of 0.74 mM for VPA in MCF-7 cells and of 1.58 mM for this drug in MDA-MB-231 cells (using 3×10^3 cells for eight days)⁴³. Moreover, this group demonstrated that VPA strongly induces apoptosis in MCF-7 cells by activating caspase 8⁴³. In the present study the IC_{50} values are lower than those indicated by Fortunati, suggesting that **2** has a greater effect on both cell lines than VPA

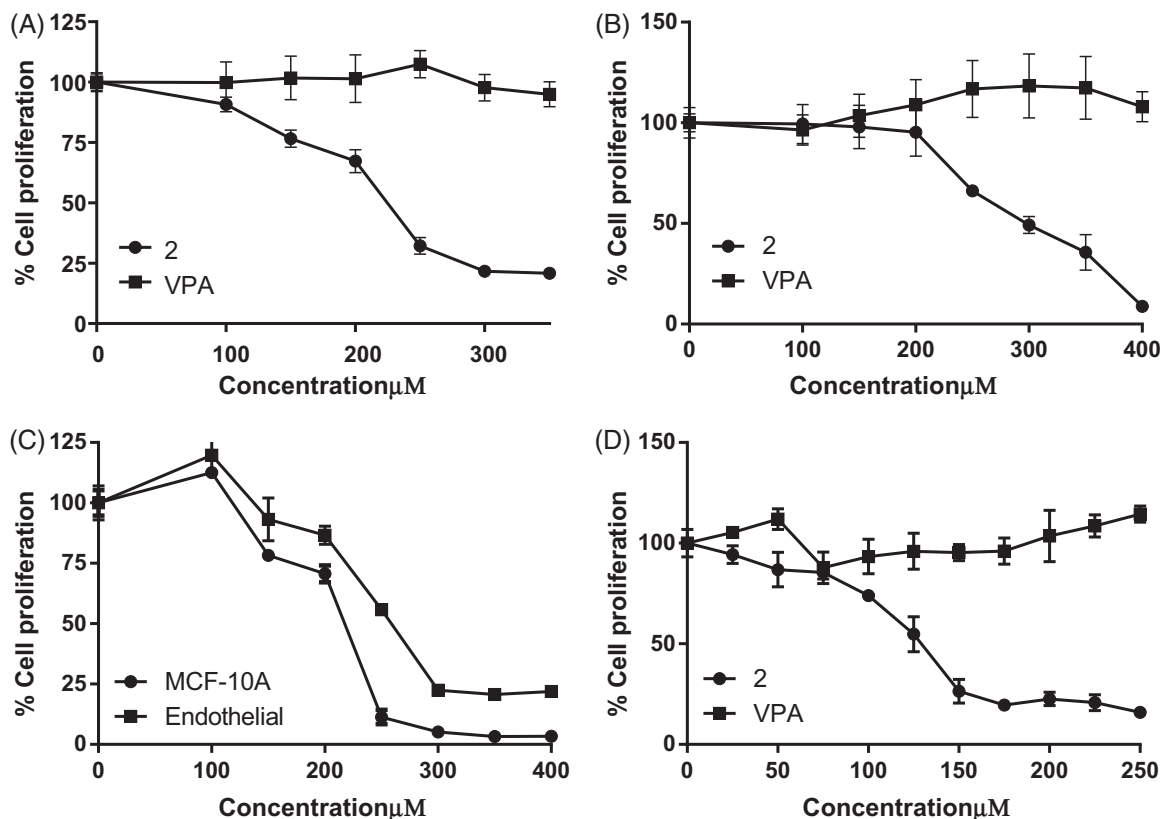


Figure 5. Effect of **2** and VPA on cell proliferation in: (A) MCF-7 cells (0–350 μM concentration of the compounds), (B) MDA-MB-231 cells (0–450 μM concentration of the compounds), (C) MCF-10A and endothelial cells (0–400 μM concentration of **2**, and (D) SKBr3 cells (0–250 μM concentration of the compounds). All data on cell proliferation after treatment are expressed as the percentage of cell growth of treated versus untreated (control) cells. All assays were determined by MTT. Results are expressed as the mean \pm SD of three independent experiments ($n = 4$).

Table 3. IC_{50} for **2** in breast cancer cell lines and non-tumorigenic cells.

Cell estrogen receptor	MCF-7 ER+, HER2+	MDA-MB-231 ER-, HER2-	SKBr3 ER-, PR-, HER2+, GPER+	MCF-10A GPER+	Epithelial
IC_{50} (mM)	0.19	0.28	0.14	0.21	0.24

due to its ability to reach the SAHA site on HDAC8, or by acting on GPR30/GPER (a promissory target in drug design for current chemotherapy) if compound were metabolized by the CYP450 giving as result a dihydroxylated aryl moiety capable to interact with the binding site onto GPER/GPR30. In 2012, Li et al. demonstrated that concentrations of up to 3.2 mM of VPA had no effect on cell proliferation of MDA-MB-231 cells, although inhibition of cell migration was observed⁴⁴. This could explain why we did not find any changes in the proliferation of cells herein treated with VPA.

In 2011, Park et al. found that expression of HDAC4, 6 and 8 is higher in MDA-MB-231 cells than MCF-7 cells, and that these isoforms are correlated with an increased expression of metalloproteinase 9 (MMP-9), which is associated with cellular invasion⁴⁵. We observed that **2** had a significant effect on the decrease in cellular proliferation of MDA-MB-231, whose characteristics is more aggressive than MCF-7 cells.

By using *in silico* assays we demonstrated that **2** binds to HDAC8 with greater affinity than VPA, evidenced by the K_d of 0.33 μM versus 4.63 μM (**2** versus VPA, respectively), calculated from their free energy values (Table 2). These theoretical data could explain the decrease in the proliferation of cancer cells used presently.

VPA is clinically relevant because its anti-proliferative activity as an HDAC inhibitor has been recently described in breast cancer patients, finding a mean plasma concentration of 86.3 mg/mL⁴⁶. In this study VPA was administrated with hydralazine, a methylation inhibitor⁴⁶. In 2007, Münster et al. conducted a clinical phase I study with 44 patients given 160 mg/kg/day of VPA, finding various adverse effects, such as drowsiness, hyponatremia, hypocalcemia, fatigue, hallucinations, dizziness, headache or dehydration⁴⁷. They found that the recommended phase II study dose is 140 mg/kg/day for 48 h, followed by 100 mg/m² of epirubicin. There are no clinical reports in which VPA is administered as monotherapy for solid tumors. Hence, the current contribution demonstrates that the interaction of **2** with two therapeutic targets was able to inhibit cell growth with a lower concentration compared to the formerly reported combination therapy. These data suggest that compound **2** is a promissory potential anticancer drug deserving further preclinical and clinical development.

Conclusions

The chemical substitution of designed molecules that inhibit HDAC8 isoform could result in a more efficient inhibition of this

enzyme than that of the starting compounds. In the present study the compound **2** was designed and synthesized, which was the result of adding a mono-substituted aryl core at the carboxyl group of VPA to give an arylamide derivative (structural similarity with SAHA). According to theoretical results, the compound **2** apparently targets to HDAC8. Additionally, the tested compound was able to inhibit the tumor cell proliferation *in vitro* at a much lower concentration than that required for achieving the same effect with VPA.

Acknowledgements

BPM thanks CONACYT for a scholarship.

Declaration of interest

The authors have declared that no competing interests exist. The present study was supported by grants from CONACYT (CB-254600; PDCPN-782; I010/0532/2014), CYTED (214RT0842), and BEIFI SIP-COFAA of the IPN (20161383; 20160204).

References

- Lopez J, Percharde M, Coley HM, et al. The context and potential of epigenetics in oncology. *Br J Cancer* 2009;100:571–7.
- Stewart BW, Wild CP. *World Cancer Report 2014*. International Agency for Research on Cancer. Geneva: WHO.
- Birch JM, Marsden HB, Morris Jones PH, et al. Improvements in survival from childhood cancer: results of a population based survey over 30 years. *Br Med J (Clin Res Ed)* 1988;296:1372–6.
- Boschmonar MG, Alvarez YG, García AM, et al. Childhood cancer survival in Cuba. *Eur J Epidemiol* 2000;16:763–7.
- Madhusoodhan PP, Carrol WL, Bhatla T. Progress and prospects in pediatric leukemia. *Curr Probl Pediatr Adolesc Health Care* 2016; 16:30015–23.
- Pearson AD, Herold R, Rousseau R, et al. Implementation of mechanism of action biology-driven early drug development for children with cancer. *Eur J Cancer* 2016;62:124–31.
- Gunjan A, Paik J, Verreault A. Regulation of histone synthesis and nucleosome assembly. *Biochimie* 2005;87:625–35.
- Biel M, Wascholowski V, Giannis A. Epigenetics-an epicenter of gene regulation: histones and histone-modifying enzymes. *Angew Chem Int Ed Engl* 2005;44:3186–216.
- Jones PL, Veenstra GJ, Wade PA. Methylated DNA and MeCP2 recruit histone deacetylase to repress transcription. *Nat Genet* 2010; 19:187–97.
- Finnin MS, Donigian JR, Cohen A, et al. Structures of a histone deacetylase homologue bound to the TSA and SAHA inhibitors. *Nature* 1999;401:188–93.
- Sixto-López Y, Gómez-Vidal JA, Correa-Basurto J. Exploring the potential binding sites of some known HDAC inhibitors on some HDAC8 conformers by Docking studies. *Appl Biochem Biotechnol* 2014;173:1907–26.
- Cameron EE, Bachman KE, Myohanen S, et al. Synergy of demethylation and histone deacetylase inhibition in the re-expression of genes silenced in cancer. *Nat Genet* 1999;21:103–7.
- Zhu WG, Otterson GA. The interaction of histone deacetylase inhibitors and DNA methyltransferase inhibitors in the treatment of human cancer cells. *Curr Med Chem Anticancer Agents* 2003;3: 187–99.
- Lindemann JRK, Gabrielli B, Johnstone RW. Histone-deacetylase inhibitors for the treatment of cancer. *Cell Cycle* 2004;3:779–88.
- Johannessen CU, Johannessen SI. Valproate: past, present, and future. *CNS Drug Rev* 2003;9:199–216.
- Chakrabarti A, Oehme I, Witt O, et al. HDAC8: a multifaceted target for therapeutic interventions. *Trends Pharmacol Sci* 2015;36: 481–92.
- Eyal S, Yagen B, Shimshoni J, Bialer M. Histone deacetylases inhibition and tumor cells cytotoxicity by CNS-active VPA constitutional isomers and derivatives. *Biochem Pharmacol* 2005;69:1501–8.
- Dowdell SKC, Pesnicak L, Hoffmann V, et al. Valproic acid (VPA), a histone deacetylase (HDAC) inhibitor, diminishes lymphoproliferation in the Fas-deficient MRL/lpr(–/–) murine model of autoimmune lymphoproliferative syndrome (ALPS). *Exp Hematol* 2009;37:487–94.
- Krämer OH, Zhu P, Ostendorff HP, et al. The histone deacetylase inhibitor valproic acid selectively induces proteasomal degradation of HDAC2. *Embo J* 2003;22:3411–20.
- Takai N, Desmond JC, Kumagai T, et al. Histone deacetylase inhibitors have a profound antigrowth activity in endometrial cancer cells. *Clin Cancer Res* 2004;10:1141–9.
- Göttlicher M. Valproic acid: an old drug newly discovered as inhibitor of histone deacetylases. *Ann Hematol* 2004; 83:S91–2.
- De Souza C, Chatterji BP. HDAC inhibitors as novel anti-cancer therapeutics. *Recent Pat Anticancer Drug Discov* 2015;10: 145–62.
- Wang ZT, Chen ZJ, Jiang GM, et al. Histone deacetylase inhibitors suppress mutant p53 transcription via HDAC8/YY1 signals in triple negative breast cancer cells. *Cell Signal* 2016;28: 506–15.
- Hsieh CL, Ma HP, Su CM, et al. Alterations in histone deacetylase 8 lead to cell migration and poor prognosis in breast cancer. *Life Sci* 2016;151:7–14.
- Rosales-Hernández MC, Bermudez-Lugo J, Garcia JA, et al. Molecular modeling applied to anti-cancer drug development, anticancer. *Agents Med Chem* 2009;9:230–8.
- Frisch MJ, Trucks GW, Schlegel HB, et al. *Gaussian 98*, Revision A.9. Pittsburgh, PA: Gaussian, Inc; 1998.
- Phillips JC, Braun R, Wang W, et al. Scalable molecular dynamics with NAMD. *J Comput Chem* 2005;26:1781–802.
- Ryckaert JP, Cicotti G, Berendsen HJC. Numerical integration of the cartesian equations of motion of a system with constraints: molecular dynamics of n-alkanes. *J Comput Phys* 1977; 23:327–41.
- Morris GM, Goodsell DS, Halliday RS, et al. Automated docking using a Lamarckian genetic algorithm and an empirical binding free energy function. *J Comp Chem* 1998;19:1639–62.
- Sheldrick G, Blessing RH. An empirical correction for absorption anisotropy. *Acta Cryst* 1995;A51:33–8.
- Sheldrick GM. A short history of SHELX. *Acta Cryst* 2008;64: 112–22.
- Farrugia LJ. *WinGX* suite for small-molecule single-crystal crystallography. *J Appl Cryst* 1999;32:837–8.
- Spek AL. *PLATON*, Version of March 2002. Heidelberglaan, The Netherlands: University of Utrecht; 2002.
- Macrae CF, Edgington PR, McCabe P, et al. Mercury: visualization and analysis of crystal structures. *J Appl Crystallogr* 2006;39: 453–7.
- Jaffe EA. *Culture and identification of large vessel endothelial cells. Biology of endothelial cells*. Boston, MA: Martinus Nijhoff; 1984:1–13.
- Achenbach J, Klinger FM, Blöcher R, et al. Exploring the chemical space of multitarget ligands using aligned self-organizing maps. *ACS Med Chem Lett* 2013;4:1169–72.
- Bermúdez-Lugo JA, Perez-Gonzalez O, Rosales-Hernández MC, et al. Exploration of the valproic acid binding site on histone deacetylase 8 using docking and molecular dynamic simulations. *J Mol Model* 2012;18:2301–10.
- Phiel CJ, Zhang F, Huang EY, et al. Histone deacetylase is a direct target of valproic acid, a potent anticonvulsant, mood stabilizer, and teratogen. *J Biol Chem* 2001;276:36734–41.
- Vannini A, Volpari C, Gallinari P, et al. Substrate binding to histone deacetylases as revealed by crystal structure of HDAC8-substrate complex. *EMBO Rep* 2007;8:879–84.
- Zang LL, Wang XJ, Li XB, et al. SAHA-based novel HDAC inhibitor design by core hopping method. *J Mol Graph Model* 2014; 54:10–18.
- Vannini A, Volpari C, Filocamo G, et al. Crystal structure of a eukaryotic Zn-dependent histone deacetylase, human HDAC8, complexed with a hydroxamic acid inhibitor. *Proc Natl Acad Sci U S A* 2004;101:15064–9.
- Dejligbjerg M, Grauslund M, Litman T, et al. Differential effects of class I isoform histone deacetylase depletion and enzymatic inhibition by belinostat or valproic acid in HeLa cells. *Mol Cancer* 2008;7:1–12.

43. Fortunati N, Bertino S, Costantino L, et al. Valproic acid is a selective antiproliferative agent in estrogen-sensitive breast cancer cells. *Cancer Lett* 2008;259:156–64.
44. Li GF, Qian TL, Li GS, et al. Sodium valproate inhibits MDA-MB-231 breast cancer cell migration by upregulating NM23H1 expression. *Genet Mol Res* 2012;11:77–86.
45. Park SY, Jun JA, Jeong KJ, et al. Histone deacetylases 1, 6 and 8 are critical for invasion in breast cancer. *Oncol Rep* 2011;25:1677–81.
46. Candelaria M, Gallardo-Rincón D, Arce C, et al. A phase II study of epigenetic therapy with hydralazine and magnesium valproate to overcome chemotherapy resistance in refractory solid tumors. *Ann Oncol* 2007;18:1529–38.
47. Münster P, Marchion D, Bicaku E, et al. Phase I trial of histone deacetylase inhibition by valproic acid followed by the topoisomerase II inhibitor Epirubicin in advanced solid tumors: a clinical and translational study. *J Clin Oncol* 2007;25:1979–85.